



## OPEN ACCESS

## EDITED BY

Shiping Wen,  
University of Technology Sydney,  
Australia

## REVIEWED BY

Pradeep Vishnuram,  
SRM Institute of Science and Technology,  
India  
Minh Quan Duong,  
The University of Danang, Vietnam  
Nirna Rezaei,  
Lakehead University, Canada

## \*CORRESPONDENCE

Paresh Kumar Nayak,  
✉ paresh@iitism.ac.in

## SPECIALTY SECTION

This article was submitted  
to Smart Grids,  
a section of the journal  
Frontiers in Energy Research

RECEIVED 10 January 2023

ACCEPTED 06 March 2023

PUBLISHED 24 March 2023

## CITATION

Prabhu MS, Biswas S, Nayak PK,  
Abdelaziz A and El-Shahat A (2023), An  
intelligent protection scheme for series-  
compensated transmission lines  
connecting large-scale wind farms.  
*Front. Energy Res.* 11:1141235.  
doi: 10.3389/fenrg.2023.1141235

## COPYRIGHT

© 2023 Prabhu, Biswas, Nayak, Abdelaziz  
and El-Shahat. This is an open-access  
article distributed under the terms of the  
[Creative Commons Attribution License  
\(CC BY\)](https://creativecommons.org/licenses/by/4.0/). The use, distribution or  
reproduction in other forums is  
permitted, provided the original author(s)  
and the copyright owner(s) are credited  
and that the original publication in this  
journal is cited, in accordance with  
accepted academic practice. No use,  
distribution or reproduction is permitted  
which does not comply with these terms.

# An intelligent protection scheme for series-compensated transmission lines connecting large-scale wind farms

M. S. Prabhu<sup>1</sup>, Sauvik Biswas<sup>2</sup>, Paresh Kumar Nayak<sup>3\*</sup>,  
Almoataz Abdelaziz<sup>4</sup> and Adel El-Shahat<sup>5</sup>

<sup>1</sup>Electrical and Electronics Engineering, Vel Tech Rangarajan Dr Sagunthala R&D Institute of Science and Technology, Chennai, India, <sup>2</sup>Electrical Engineering, Indian Institute of Technology, Delhi, India, <sup>3</sup>Electrical Engineering, Indian Institute of Technology (ISM), Dhanbad, India, <sup>4</sup>Faculty of Engineering and Technology, Future University in Egypt, Cairo, Egypt, <sup>5</sup>Energy Technology Program, School of Engineering Technology, Purdue University, West Lafayette, IN, United States

Series-compensated transmission lines (SCTLs) are increasingly preferred for transmitting bulk amounts of electricity generated from the present-day large-scale wind farm to the utility grid due to several technical and economic benefits. However, when a fault occurs in such a wind farm-integrated SCTL, the impedance across the metal oxide varistor (MOV)-protected series capacitor varies non-linearly. Also, the fault current contributed from the wind farm side is quite different compared to the grid side. Consequently, the widely used fixed impedance-based distance relaying schemes showed limitations when used for protecting such crucial TLs. In this paper, the impacts of series compensation and wind farm integration on distance relay are investigated, and this paper proposes an intelligent relaying scheme using only the current measurements. In the proposed scheme, the fault detection task is performed using the signs of the half-cycle magnitude differences of the line end positive-sequence currents, and the fault classification task is performed using only the local current measurements processed through the Fourier–Bessel series expansion (FBSE) bagging ensemble (BE) classifier. The non-stationary components present in the current signal at the initiation of a fault are captured by calculating FBSE coefficients, and the singular value decomposition is applied for dimensionality reduction of the feature set. Finally, the extracted features are used by the BE classifier for fault classification. The method is evaluated in MATLAB/Simulink® on numerous fault and non-fault data simulated in two-bus systems and also validated through the OPAL-RT (OP4510) manufactured real-time digital simulation platform. The obtained results (response time for fault detection and classification <10 ms), including the comparative assessment results (fault detection accuracy = 100% and fault classification accuracy = 99.37%), justify the effectiveness of the proposed relaying scheme in protecting the wind farm-integrated SCTLs.

## KEYWORDS

series-compensated transmission line, DFIG-WTG, large-scale wind farm, distance relay, fault detection, fault classification, bagging ensemble classifier

# 1 Introduction

## 1.1 Background and motivation of the research

In recent years, a considerable growth has been observed in electricity generation using wind energy across the world (Chaurasiya et al., 2019). Currently, the doubly fed induction generator (DFIG) is one of the most accepted wind turbine generators (WTGs) due to its various technical and economic advantages (Lopez et al., 2007). The large-scale DFIG-based wind farms are usually integrated to the utility grid through high-voltage transmission lines (HV-TLs). However, the restrictions on building new transmission facilities due to environmental and economic reasons impose main barriers in harnessing the full potential of the wind energy. To get rid of the problem, series-compensated transmission lines (SCTLs) are increasingly preferred nowadays for transmitting the bulk amount of electricity generated from large-scale wind farms to the utility grid (Varma et al., 2008), (Varma and Moharana, 2013). However, the power electronics interfaced distributed energy resources, especially large-capacity solar photovoltaic plants (Hoang et al., 2022) or large-capacity DFIG-WTGs with low-voltage ride through (LVRT) capability (Li et al., 2018), have quite unusual fault patterns compared to conventional synchronous generators. Also, the non-linear functioning of the metal oxide varistor (MOV) protecting the series capacitor produces unusual fault currents and causes rapid variation in the line impedance, especially during the first one or two cycles after the initiation of the faults. Consequently, the widely used fixed impedance-based distance relaying schemes, when used for protecting such wind farm integrated SCTLs, show limitations in providing fast and reliable protection. Motivated by the previous issues, an improved relaying scheme is proposed in this paper with an intention of ensuring fast and reliable protection to SCTL connecting large-scale DFIG-based wind farms.

## 1.2 Literature review

In the last decade, several improved relaying schemes were reported in the literature in order to provide fast and reliable protection to large-scale DFIG-based wind farm-integrated HV-TLs compensated with/without series capacitors. The merits and demerits of each of the available methods are discussed in the following.

The detailed theoretical analysis of the dynamic behavior of the DFIG during symmetrical and asymmetrical voltage sags is studied by Lopez et al. (2007) and Ouyang and Xiong (2014) and Lopez et al. (2008) and Xiao et al. (2015), respectively. It is demonstrated that asymmetrical voltage sags are more dangerous than symmetrical voltage sags. Different adaptive trip boundary-setting techniques are proposed for distance relays protecting DFIG-based wind farm-connected TLs (Pradhan and Joos, 2007; Sadeghi, 2012; Dubey et al., 2014; Chen et al., 2017a; Ma et al., 2018; Prasad and Biswal, 2020; Prasad et al., 2020). In the study by Sadeghi (2012), an adaptive trip boundary-setting technique is proposed for distance relay protecting a wind farm-connected TL using an artificial neural network (ANN).

In that scheme, line impedance is estimated using the wind farm-side voltage and current measurements first and then trained using a scaled conjugate gradient backpropagation technique. However, to obtain higher accuracy, a large dataset is built for the ANN. The adaptive distance relay setting for the line connecting the wind farm is proposed by Dubey et al. (2014). Line-end voltage and current signals are used for adaptive trip boundary setting. However, no information is provided about the type of generator and related wind farm control and protection strategies.

In Chen et al. (2017a), zone-2 of the distance relay is set adaptively using an adaptive branch coefficient according to the fault type and equivalent sequence impedances of WTGs. Another adaptive distance protection scheme is proposed by Ma et al. (2018) to protect low-voltage collector lines of DFIG-based wind farms using the phase relationship of the fault current. Recently, swarm intelligence-assisted adaptive threshold-based differential protection schemes have been proposed by Prasad and Biswal (2020), (Prasad et al., 2020), to protect DFIG wind farm-integrated TLs. However, all the previously conducted studies for adaptive distance relay settings are not specific to the fault characteristics of DFIG-WTGs and mostly require line-end voltage and current measurements to implement the adaptive protection schemes. The other protection schemes such as the time-domain-based distance relaying algorithm (Lopez et al., 2007), modified permissive overreach transfer trip method (Hooshyar et al., 2014), unit protection scheme (Ghorbani et al., 2017), transient-based distance protection scheme (Chen et al., 2017b), zero-sequence impedance-based relaying algorithm (Fang et al., 2018), and wavelet transform (WT)-based protection approach (Yang et al., 2020) are also proposed for the protection of DFIG-based wind farm-connected TLs.

The limitations of distance relay protecting SCTLs are documented in several research articles (Novosel et al., 1997; Altuve et al., 2009; Vyas et al., 2014; Hoq et al., 2021). Furthermore, newer solutions are reported in the literature to ensure improved protection for such SCTLs (Abdelaziz et al., 2005; Dash et al., 2006; Nayak et al., 2014; Mishra et al., 2019). Only (Sivov et al., 2016; Sahoo and Samantaray, 2017; Mishra et al., 2021; Mohamed et al., 2021), improved protection schemes are proposed for SCTLs (compensated with either a fixed series capacitor (FSC) or a thyristor-controlled series capacitor (TCSC)) connected with large-scale wind farms. In the study by Sivov et al. (2016), an adaptive zone setting method is proposed for the distance relay protecting a fixed series capacitor-compensated transmission line connected to the wind power plant. However, for the implementation of the adaptive setting, the method requires both end voltage and current measurements and current measurements before and after the series compensation. Thus, it requires a dedicated communication medium for implementation of the protection scheme. In the study by Sahoo and Samantaray (2017), a protection solution is proposed for TCSC-compensated lines connecting DFIG-based wind farms using line-end synchronized voltage and current measurements at a sampling frequency of 200 kHz. From a practical implementation point of view, such a high-frequency sampling may not be economically attractive. Another adaptive distance relaying scheme is proposed recently by Mohamed et al. (2021) for fast and reliable protection of TCSC-compensated HV-TL connecting wind farms using line-end voltage and current measurements received through a limited

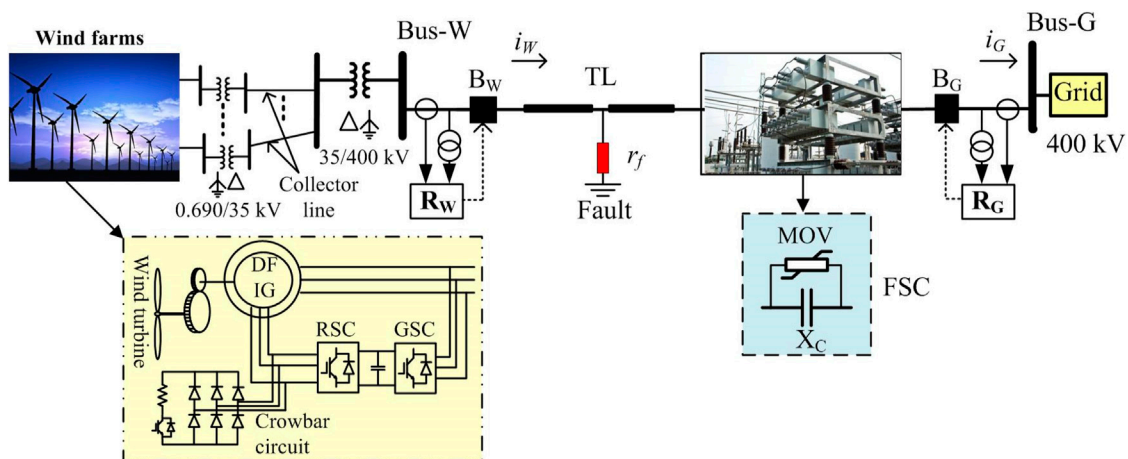


FIGURE 1

Single-line diagram of a two-bus test power system (in this study, the zone-1 reach of  $R_W$  and  $R_G$  is set equal to 80% length of the TL).

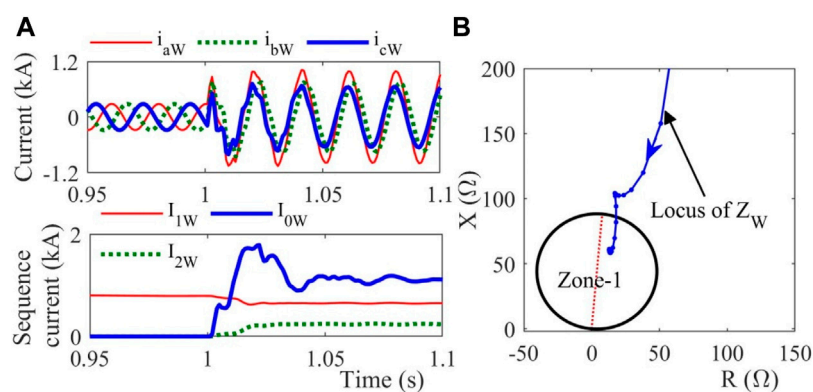


FIGURE 2

Demonstration of the impacts of unbalanced ground faults (cg-type) on relay  $R_W$  protecting the large-scale DFIG wind farm-connected TL.

communication facility. Another traveling wave-based fault location technique is proposed by Mishra et al. (2021) for an FSC-compensated TL connecting DFIG-based wind farm using line-end voltage measurements at a sampling frequency of 1,000 kHz.

The aforementioned study clearly shows that, in most of the published papers, the fault behaviors of large-scale DFIG-based wind farms and their impacts on distance relaying-based TL protection schemes are studied thoroughly and demonstrated through simulation results. Similarly, several articles are reported to provide enhanced protection to SCTLs. However, except a few, none of the methods have studied the simultaneous impacts of the integration of DFIG-based wind farms and series compensation on distance relaying-based TL protection schemes. Also, the relaying schemes proposed for improved protection of DFIG-based wind farm-integrated FSC/TCSC-compensated HV-TL require both end voltage and current measurements. Thus, efficacies of the available methods depend very much on the communication medium. Also, some of the schemes require data at a very high sampling frequency. Thus, from a practical implementation point of view, the available methods will be costlier.

Hence, an economically feasible improved protection scheme is very much essential at this point for effective protection of the SCTL connecting large-scale DFIG-based wind farms.

### 1.3 Contribution and paper organization

In this paper, a new intelligent fault detection and classification technique is proposed for an FSC-compensated TL connecting large-scale DFIG-based wind farms. The main contributions including the novelty of the present work are highlighted as follows:

- The impacts of FSC compensation and DFIG-based wind farm integration on the performance of the distance relay are investigated rigorously through both analytical study and simulation results
- The use of the sign of the half-cycle magnitude difference of the line-end positive-sequence currents for fast and accurate detection of faults in the DFIG-based wind farm-integrated

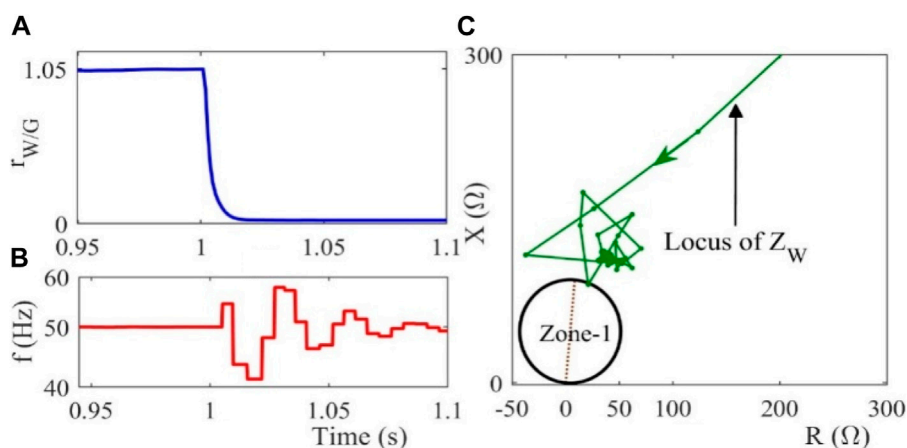


**FIGURE 3**  
Demonstration of the impacts of three-phase faults on the performance relay  $R_W$  protecting the large-scale DFIG wind farm-connected TL.

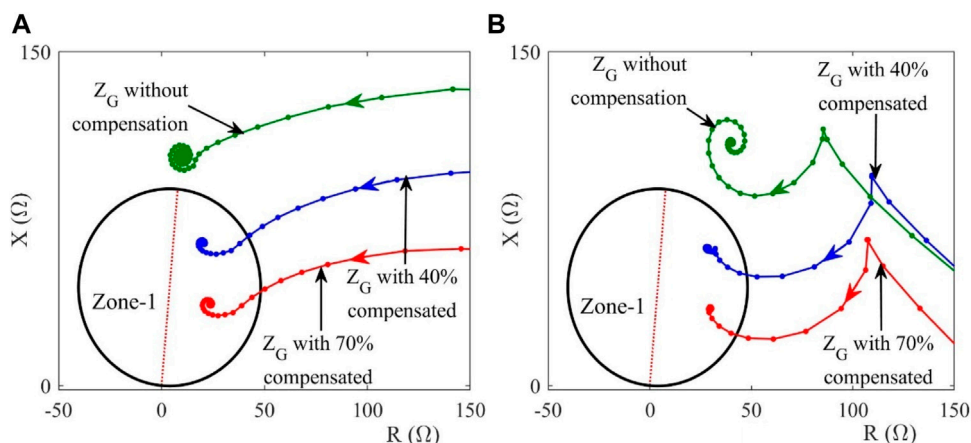


**FIGURE 4**  
Demonstration of the impacts of balanced and unbalanced ground faults on relay  $R_G$  during (A) abc-g-fault and (B) ag-fault.

FSC-compensated TL is the main novelty and contribution of the present work

- The extraction of useful features from the grid-side measured currents using an efficient time-frequency signal processing technique known as Fourier–Bessel series expansion (FBSE) and an efficient matrix decomposition technique, namely, the singular value decomposition (SVD), and furthermore, fast and accurate classification of the fault using a bagging ensemble classifier is another novelty and the second main contribution of the present work
- Validation and implementation of the proposed method through MATLAB/Simulink® and OPAL-RT (OP4510)-manufactured real-time digital simulation (RTDS) platforms on numerous fault and non-fault data simulated in a two-bus test system are another contribution of the present work

The rest of this paper is organized as follows. The impacts of the installation of FSC compensation and integration of DFIG-based

windfarms on the conventional distance relay are investigated in detail in Section 2. The proposed fault detection and classification technique is elaborated in Section 3. Results and discussions and comparative results are provided in Sections 4 and Section 5, respectively. Validation of the proposed protection scheme in the RTDS platform is demonstrated in Section 6. Finally, the conclusion of the paper is provided in Section 7.

## 2 Protection challenges of FSC-compensated TLs connecting large-scale wind farms

The two-bus system, as shown in Figure 1, is simulated in MATLAB/Simulink® for evaluating the impacts of the FSC compensation and wind farm integration on distance relays. Specifications of each of the system components are provided in Appendix. As shown in the figure, the crowbar circuit is

installed on the rotor side of the DFIG-WTG to protect the rotor-side converter (RSC) during grid voltage sags. The wind farm with LVRT capability acts as a weak power system compared to the utility grid. Different converters (Nayak et al., 2022) and optimization techniques (Vishnuram et al., 2021) are considered for the study. In the present research, the large capacity DFIG-WTG satisfies LVRT capability during grid faults as per the requirement of the Indian grid code (Central Electricity Regulatory Commission, 2010). The DFIG-WTG with LVRT capability produces unusual sequence currents that generally affect the performance of the wind farm-side distance relay  $R_W$  (Lopez et al., 2007), (Pradhan and Joos, 2007). Furthermore, as series compensation is provided at the grid side of the line, the non-linear operation of the MOV protecting the series capacitor during a fault in the TL will result in a non-linear variation of the line impedance (Novosel et al., 1997; Abdelaziz et al., 2005; Altuve et al., 2009; Vyas et al., 2014; Hoq et al., 2021). Thus, it will affect the performance of the grid-side distance relay  $R_G$ . Therefore, the performance of both-side distance relays needs to be tested.

## 2.1 Impact study on wind farm-side relay $R_W$

The wind farm is usually connected to the grid through a star-grounded HV transformer, as shown in Figure 1. As the wind farm side is delta connected, it restricts the flow of zero-sequence current when a ground fault occurs in the interconnected TL. The zero-sequence current of the ground fault is limited only by the zero-sequence impedance of the HV transformer and the TL. Thus, higher magnitudes of zero-sequence current than positive- and negative-sequence currents exist as the wind farm side acts as a weak power supply system. The unusual sequence components of current during ground fault and the control action of the DFIG-WTGs with LVRT capability affect the performance of wind farm-side distance relay  $R_W$ .

To test the performance of relay  $R_W$  of Figure 1 during ground faults, a cg-fault ( $r_f = 10 \Omega$ ) is started at 1 s on the 400-kV line at a distance of 270 km (90% length of the line) from  $R_W$  with a wind speed  $v = 15$  m/s and an FSC compensation level ( $CL$ ) = 40%. The result for the fault case is shown in Figure 2. As shown in Figure 2A, the magnitude and wave shape of phase-c current and the sequence currents produced are pretty unusual due to the grounding arrangements and control actions of the DFIG-WTGs. Due to the high magnitude of zero-sequence current and the limited increase in fault current magnitude of phase-c, the impedance  $Z_W (= \bar{V}_{cW}/(\bar{I}_{cW} + k_0 \bar{I}_{0W}))$ , where  $\bar{V}_{cW}$  and  $\bar{I}_{cW}$  are the voltage and current phasors of phase-c;  $k_0$  is the residual compensation factor; and  $\bar{I}_{0W}$  is the zero-sequence current) seen at relay  $R_W$  is reduced compared to the impedance between the relay and the fault point. As a result, even if the fault has occurred outside of zone-1, the impedance seen at relay  $R_W$  enters its zone-1 characteristics. A similar result is also obtained for other types of ground faults. This shows that when used to protect TLs connecting large-scale DFIG-WTGs, the conventional distance relay will face an overreaching problem.

The apparent impedance  $Z_W$  seen at relay  $R_W$  (Figure 1) during a balanced three-phase fault can be computed as (Biswas and Nayak, 2021a)

$$Z_W = \frac{\bar{V}_W}{\bar{I}_W} = (Z_{Wf} + r_f) + \frac{r_f}{r_{W/G}} \quad (1)$$

where  $r_{W/G} = \bar{I}_W/\bar{I}_G$ . During faults in the interconnected TL, the contribution of current from the wind farm side is relatively low compared to the grid side due to the control action and weak system of the DFIG-WTG causing  $r_{W/G} \ll 1$ . As a result, the impedance seen at relay  $R_W$  due to even low fault resistance  $r_f$  is magnified, which may impose an underreach problem on  $R_W$ .

To test the performance of  $R_W$ , the result of a three-phase fault ( $r_f = 5 \Omega$ ) started at a distance of 210 km (70% length of the TL) from  $R_W$  with  $v = 15$  m/s is shown in Figure 3. As observed in Figure 3A, during steady-state,  $r_{W/G} \cong 1$  shows the power flow from the wind farm to the utility grid. However, at the inception of a three-phase fault at 1 s,  $r_{W/G} \ll 1$  due to a significantly high contribution of  $\bar{I}_G$  compared to  $\bar{I}_W$ . Also, the control action of DFIG-WTG produces subharmonics apart from the fundamental frequency component, which is evident from Figure 3B. The low current contribution from the wind side and high fluctuations in the frequency components introduce errors in the impedance calculation at relay  $R_W$ , resulting in underreach problems evident in Figure 3C.

## 2.2 Impact study on grid-side relay $R_G$

As in Figure 1, series compensation in the fault loop affects the apparent impedance measured by grid-side distance relay  $R_G$ . The apparent impedance  $Z_G$  measured at relay  $R_G$  for different faults (abc/abcg, ag, and ab/bag types) when occurring at  $F$  (Figure 1) can be computed as (Biswas and Nayak, 2019)

$$Z_G(abcg) = \frac{\bar{V}_{G1}}{\bar{I}_{G1}} = Z_{Gf} + \frac{\bar{V}_{FSC1}}{\bar{I}_{G1}} + \frac{\bar{I}_{f1} r_f}{\bar{I}_{G1}} \quad (2)$$

$$Z_G(ag) = \frac{\bar{V}_{Ga}}{\bar{I}_{Ga} + k_0 \bar{I}_{G0}} = Z_{Gf} + \frac{\bar{V}_{FSCa}}{\bar{I}_{Ga} + k_0 \bar{I}_{G0}} + \frac{\bar{I}_{fa}}{\bar{I}_{Ga} + k_0 \bar{I}_{G0}} r_f \quad (3)$$

$$Z_G(ab/bag) = \frac{\bar{V}_{Ga} - \bar{V}_{Gb}}{\bar{I}_{Ga} - \bar{I}_{Gb}} = Z_{Gf} + \frac{\bar{V}_{FSCa} - \bar{V}_{FSCb}}{\bar{I}_{Ga} - \bar{I}_{Gb}} + \frac{\bar{I}_{fa} - \bar{I}_{fb}}{\bar{I}_{Ga} - \bar{I}_{Gb}} r_f \quad (4)$$

In (2)–(4), the voltage drops across the FSC, i.e.,  $\bar{V}_{FSC}$ , varies non-linearly, especially during the first one or two cycles after the initiation of the fault due to the non-linear functioning of the MOV protecting the FSC. As a result, relay  $R_G$  will see variable impedance at least during the first one or two cycles after the initiation of the fault, where actually the distance relay takes the decision and hence can affect the performance of  $R_G$ .

To evaluate the performance of  $R_G$ , the results of two typical fault cases are demonstrated here. The first one is a three-phase fault (abcg-type) created at 270 km (90%-line length) away from  $R_G$  while  $v = 10$  m/s and compensation levels are 40% and 70%, respectively. Results for the test cases are provided in Figure 4. It is evident from Figure 4A that the relay  $R_G$  faces an overreach problem due to the presence of series compensation in the fault loop. Another ag-fault is created, keeping the fault distance and wind speed the same. The characteristics of the relay  $R_G$  are shown in Figure 4B. In this fault case also,  $R_G$  faces an overreaching problem.

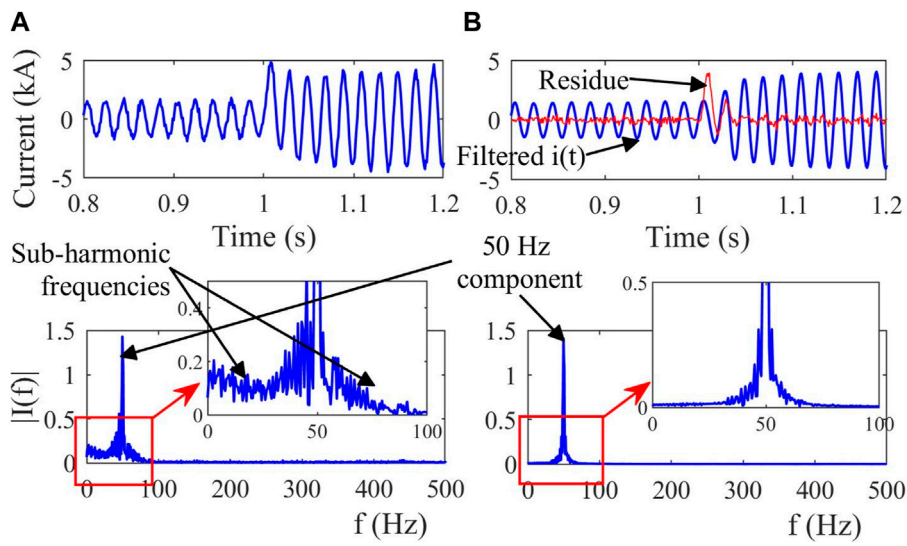


**FIGURE 5** Demonstration of the elimination of subharmonic components from the contaminated fault current signal using the Weiner filter.

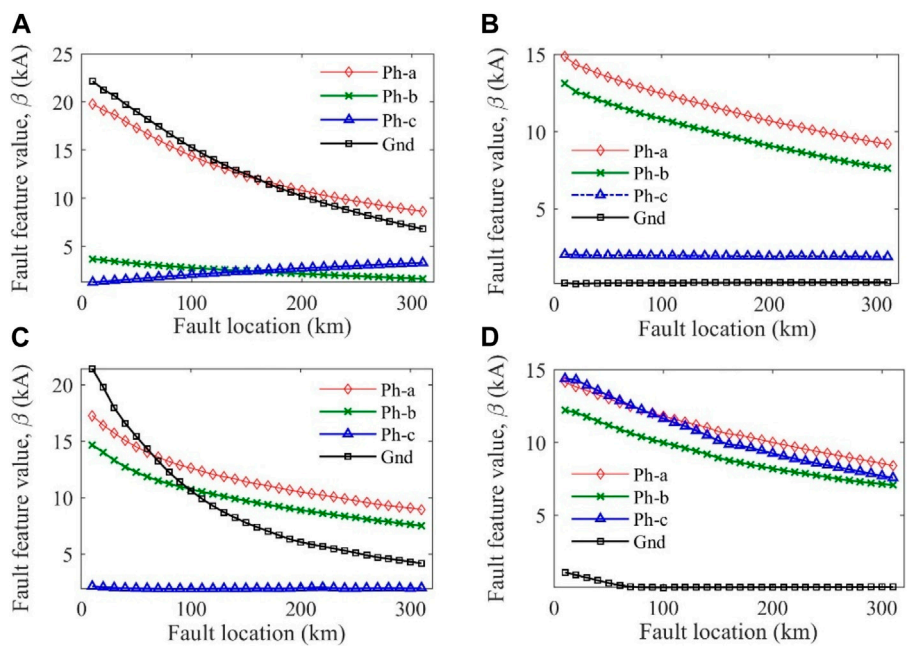


**FIGURE 6** Demonstration of the variation of fault feature  $\beta$  with fault locations for (A) ag-fault, (B) ab-fault, (C) abg-fault, and (D) abc-fault.

### 3 Proposed protection scheme

In the present work, signs of the half-cycle magnitude differences of the line end positive-sequence currents are utilized for discriminating internal faults from external faults. Furthermore, the currents measured at the utility grid side are processed through FBSE and the SVD, and finally, the BE classifier is used for fault classification. The calculation steps of the proposed fault detection

and classification scheme are provided in the following sections in detail.

#### 3.1 Proposed fault detection technique

Let the three-phase currents of the grid side and wind farm side be denoted as  $(\bar{I}_{aG}, \bar{I}_{bG}, \bar{I}_{cG})$  and  $(\bar{I}_{aW}, \bar{I}_{bW}, \bar{I}_{cW})$ ,

TABLE 1 Parameter variation for the generated 6000 possible fault cases.

Parameters	Cases	No. of cases
Fault types (FTs)	ag, bg, cg, ab, bc, ca, abg, bcg, cbg, abc.	10
Fault resistance ( $R_f$ )	1, 10, 30, 200 $\Omega$ .	4
Fault location ( $L_f$ )	20%, 40%, 60%, 80%, 100% of line length.	5
Fault inception angle (FIA)*	0°, 54°, 90°, 144°, 180°.	5
Compensation level (CL)	40%, 70%.	2
Wind speed ( $v$ )	5, 10, 15 m/s.	3
Total number of fault cases generated = $10 \times 4 \times 5 \times 5 \times 2 \times 3 = 6000$		

\*Fault inception angle is set about negative to positive zero crossing of phase-a voltage.

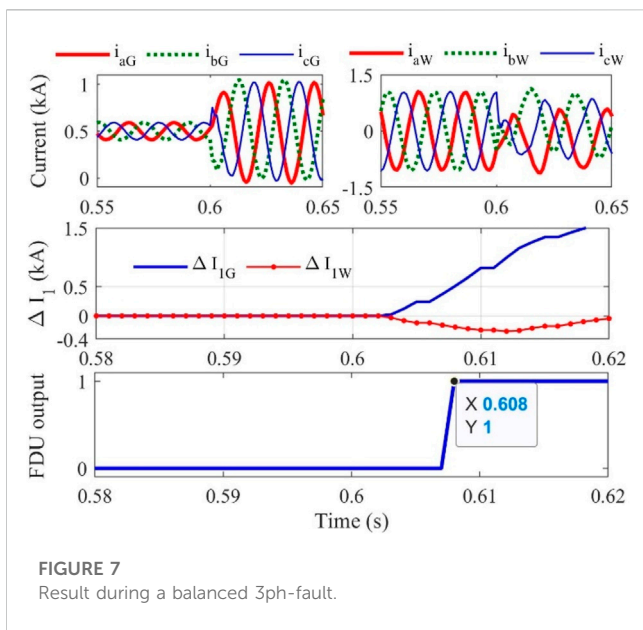


FIGURE 7 Result during a balanced 3-phase fault.

respectively. The positive-sequence currents at the grid side ( $\bar{I}_{1G}$ ) and the wind farm side ( $\bar{I}_{1W}$ ) are computed from three-phase currents using the Fortescue transform as follows (Fortescue, 1918):

$$\bar{I}_{1G} = \frac{1}{3} [\bar{I}_{aG} + \alpha \bar{I}_{bG} + \alpha^2 \bar{I}_{cG}], \bar{I}_{1W} = \frac{1}{3} [\bar{I}_{aW} + \alpha \bar{I}_{bW} + \alpha^2 \bar{I}_{cW}] \quad (5)$$

where  $\alpha = e^{j2\pi/3}$ . In the present work, phasor currents are computed from the measured time-domain currents using the full-cycle discrete Fourier transform (DFT). The half-cycle magnitude differences of the positive-sequence currents at the grid side and the wind farm side are calculated as follows (Biswas and Nayak, 2021b):

$$\begin{aligned} \Delta I_{1G}(n) &= |\bar{I}_{1G}(n)| - |\bar{I}_{1G}(n - P/2)| \text{ and } \Delta I_{1W}(n) \\ &= |\bar{I}_{1W}(n)| - |\bar{I}_{1W}(n - P/2)| \end{aligned} \quad (6)$$

where  $P$  represents the no. of samples/cycles.

It is observed from the simulation results that at the inception of an internal fault, there is a reduction in positive-sequence current magnitude from the wind farm side, whereas there is an increase in positive-sequence current magnitude from the grid side to the fault

point. Consequently, the half-cycle magnitude differences of the positive-sequence current at the wind farm side become negative just after initiating an internal fault. On the other hand, the half-cycle magnitude differences of the positive-sequence current at the grid side become positive just after initiating an internal fault. As a result, the signs of  $\Delta I_{1G}$  and  $\Delta I_{1W}$  are opposite during the inception of an internal fault. This distinguishing feature, i.e., the signs of  $\Delta I_{1G}$  and  $\Delta I_{1W}$ , is utilized in this paper for discriminating internal faults from external faults and any other non-fault transients.

During steady-state system operating conditions,  $|\Delta I_{1G}| = |\Delta I_{1W}| = 0$ . However, due to frequency variations during the switching of loads, low magnitudes of  $\Delta I_{1G}$  and  $\Delta I_{1W}$  are observed. Thus, to make  $\Delta I_{1G}$  and  $\Delta I_{1W}$  zeros during normal operation/non-fault transients, a significantly small threshold  $\epsilon = 0.005$  is set as

$$\Delta I_{1G}, \Delta I_{1W} = \begin{cases} 0; & |\Delta I_{1G}| = |\Delta I_{1W}| < \epsilon \\ \Delta I_{1G}, \Delta I_{1W}; & \text{otherwise} \end{cases} \quad (7)$$

Thus, the proposed fault detection unit (FDU) detects a fault when the criterion in (8) is satisfied.

$$\text{sign}(\Delta I_{1G}) \neq \text{sign}(\Delta I_{1W}) \rightarrow \text{FDU output} = 1 \quad (8)$$

Elimination of noise and subharmonics from the fault current signals using the Wiener filter

The use of anti-aliasing filters in DFT restricts the noise in the fault current signals. However, the DFT has a limitation in eliminating subharmonic components generated in the wind farm-side fault current due to the control actions of the DFIG. In this work, the Wiener filter removes subharmonics from the fault current (Tikhonov, 1963). Let an observed signal  $i(t)$  consisting of an original signal  $i_o(t)$  with additive zero-mean Gaussian noise  $\eta$  be expressed as follows:

$$i(t) = i_o(t) + \eta \quad (9)$$

Using Tikhonov regularization,  $i_o(t)$  is recovered by the ill-posed inverse method as follows (Tikhonov, 1963):

$$\min_{i_o} \{ \|i_o - i\|_2^2 + \alpha \|\partial_t i_o\|_2^2 \} \quad (10)$$

where  $\alpha$  is the variance of noise  $\eta$ . The Euler–Lagrange equations are solved in the Fourier domain as follows:

$$\mathcal{F}\{i(\omega)\} = i / (1 + \alpha\omega^2) \quad (11)$$

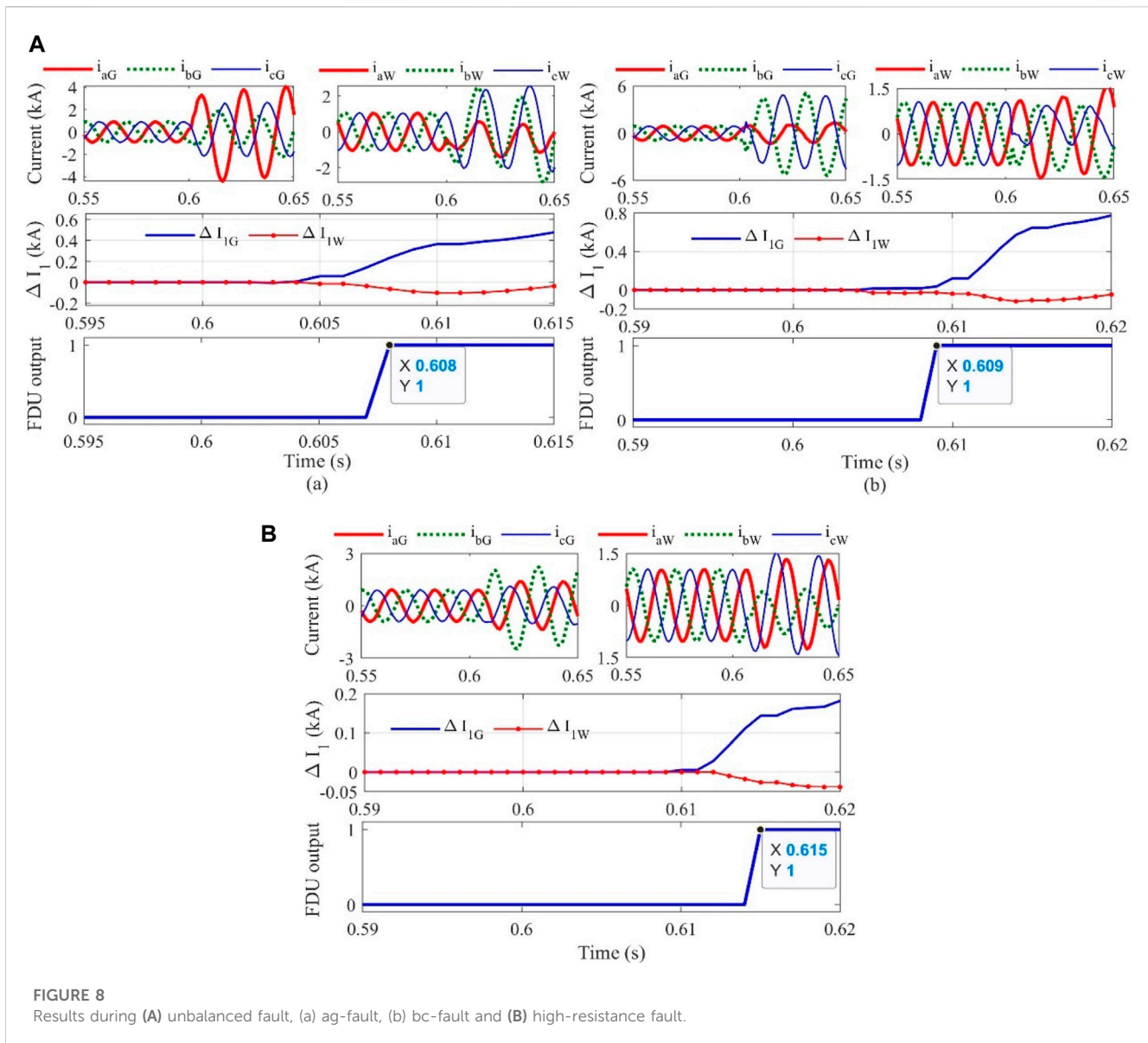


**FIGURE 8**  
Results during (A) unbalanced fault, (a) ag-fault, (b) bc-fault and (B) high-resistance fault.

Here, the estimated signal  $i_o$  is a low-pass narrow-band selection of  $i$  around  $\omega = 0$ . For example, a noisy current signal  $i(t)$  is chosen, and its corresponding fundamental and harmonic frequencies are shown in Figure 5A. It is evident that  $i(t)$  is suffered from dominant subharmonic noise. However, the Weiner filter removes subharmonics from the current waveform, which is clearly evident from Figure 5B.

### 3.2 Proposed fault classification technique

The FBSE is an efficient time-frequency signal processing technique widely used to analyze non-linear and non-stationary signals. The main advantage of FBSE is that it has unique coefficients for a given signal, and the Bessel functions are aperiodic and decay over time (Pachori and Sircar, 2008). The synthesized signal from the FB coefficients has an inherent filtering property that helps reduce the noise in the low- and

high-frequency regions of the spectrum. The various application areas of FBSE include speech-related applications (Gopalan, 2001), (Gopalan et al., 1997) and fault diagnosis studies (D'Elia et al., 2012), (Tran et al., 2013). In the fault diagnosis area, the FBSE and the Wigner–Ville distribution are used together to identify gear faults (D'Elia et al., 2012). Tran et al. (2013) used FBSE in association with generalized discriminant analysis and simplified fuzzy ARTMAP to diagnose induction motor faults. The mathematical backgrounds and the applicability of FBSE, SVD, and BE classifiers for TL fault classification are provided in the following.

### 3.3 Fourier–Bessel series expansion

As previously mentioned, the grid-side three-phase current signals are utilized for fault classification. Let the discrete-time-domain current signal of the grid side be denoted as  $i_C(t)$ . The FBSE



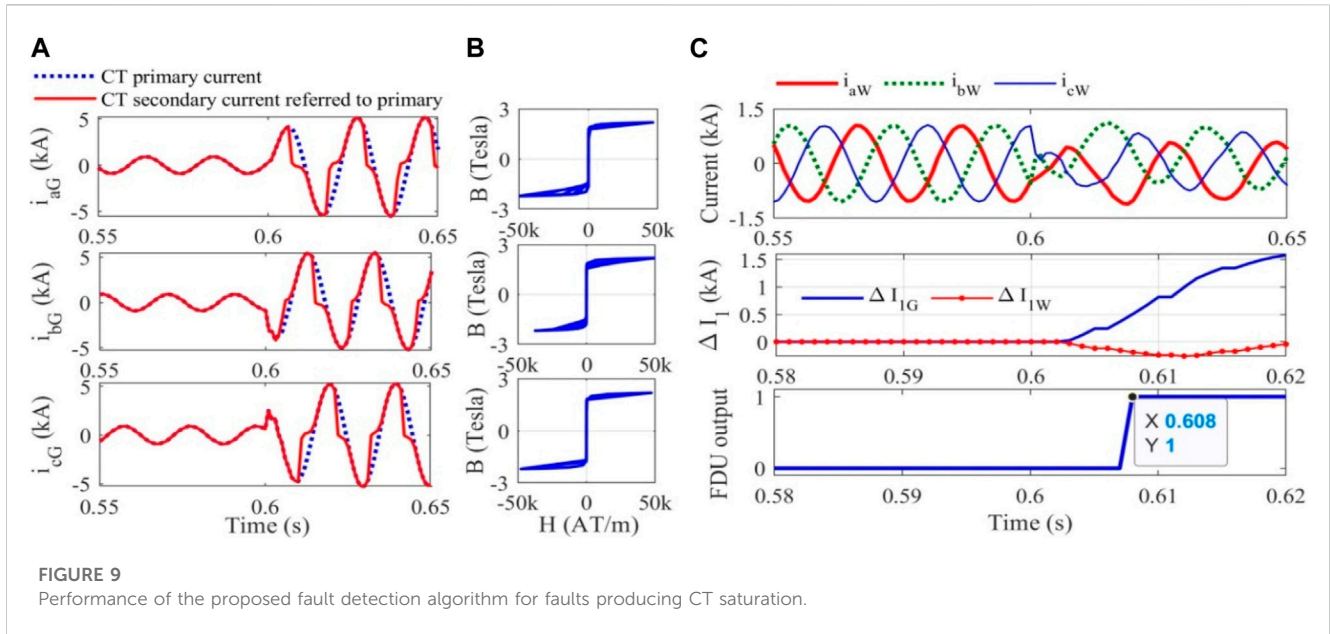


**FIGURE 9**  
Performance of the proposed fault detection algorithm for faults producing CT saturation.

of  $i_G(t)$  can be expressed using a zero-order Bessel function over some finite interval  $(0, a)$  as follows (Schroeder, 1993):

$$i_G(t) = \sum_{m=1}^M C_m J_0\left(\frac{\lambda_m t}{a}\right) \tag{12}$$

where  $J_0(\cdot)$  are the zero-order Bessel functions, which are the solution of Bessel’s differential equation.

Using the orthogonality of the set  $J_0\left(\frac{\lambda_m t}{a}\right)$ , the FB coefficient  $C_m$  is computed as follows:

$$C_m = \frac{2 \int_0^a t i_G(t) J_0\left(\frac{\lambda_m t}{a}\right) dt}{a^2 [J_1(\lambda_m)]^2} \tag{13}$$

where  $J_1(\cdot)$  are the first-order Bessel functions. The integral in the numerator in the previous equation is known as the finite Hankel transform. In this paper, the values of FB coefficients  $C_m$  computed from the grid-side measured three-phase current signals are utilized as a feature. The mathematical details of FBSE for time-frequency domain analysis are provided by Gopalan (2001), Tran et al. (2013), and Schroeder (1993).

### 3.4 Singular value decomposition

Due to dimensionality issues, the direct use of FBSE coefficients as input feature vectors is computationally expensive. The SVD is an efficient matrix decomposition technique that can effectively reduce the vectors’ dimensionality and capture the transient present in the measured time-domain signal (Pazoki, 2018). The SVD rearranges the FBSE coefficient matrix  $A_{m \times n}$  into a product of three matrices as in the following equation:

$$A_{m \times n} = U_{m \times r} \Sigma_{r \times r} V_{n \times r}^T \tag{14}$$

where  $U_{m \times r}$  is the orthogonal matrix,  $V_{n \times r}$  is the orthogonal transpose matrix, and  $\Sigma_{r \times r}$  is a diagonal matrix.  $\Sigma_{r \times r}$  is expressed as follows (Mishra et al., 2018):

$$\Sigma_{r \times r} = \begin{bmatrix} \lambda_1 & 0 & \dots & 0 & 0 \\ 0 & \lambda_2 & \dots & 0 & 0 \\ \dots & \dots & \dots & \dots & \dots \\ 0 & 0 & \dots & \lambda_{r-1} & 0 \\ 0 & 0 & \dots & 0 & \lambda_r \end{bmatrix} \tag{15}$$

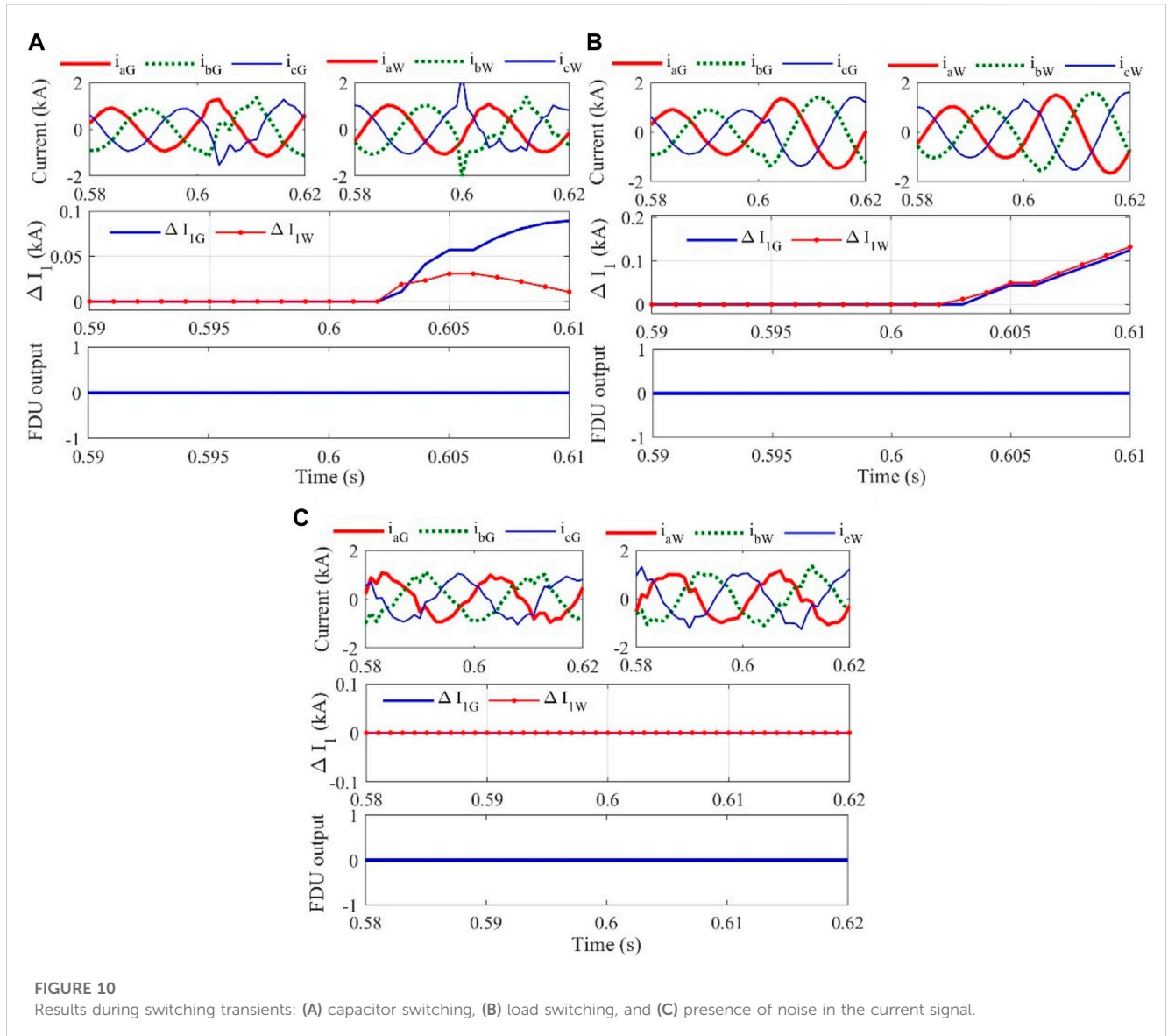
where the diagonal elements  $\lambda_i = (1, 2, \dots, r)$  are called singular values of matrix  $\Sigma_{r \times r}$ . The singular values are all non-negative real numbers and arranged in decreasing order (i.e.,  $\lambda_1 \geq \lambda_2 \geq \dots \geq \lambda_r \geq 0$ ).

In the present work, the FBSE coefficients calculated using (13) from the measured one-cycle local post-fault current signal are stored in the matrix  $A_{m \times n}$ . The high-frequency features stored in  $A_{m \times n}$  contain the maximum energy and are susceptible to any change in the signal. Consequently, the highest change will be observed in the first singular value from the primary model characteristic of the matrix  $A_{m \times n}$ . Thus, in this work, the maximum value of  $\Sigma_{r \times r}$ , i.e.,  $\beta = \max(\Sigma_{r \times r})$ , is used as the final feature for fault classification.

The variation of the amplitudes of fault feature  $\beta$  derived from the grid-side three-phase currents and the zero-sequence currents concerning the location of faults for four different fault cases, i.e., ag-, ab-, abg-, and abc-faults are shown in Figure 6. It is noticed that the faulty features have higher values than their healthy counterparts. This will enable faster fault classification through a suitable machine learning technique.

### 3.5 Bagging ensemble classifier

An ensemble-based learning algorithm has drawn considerable attention in classification and regression problems in recent years. The idea behind this learning process is to use several learners instead of a single learner and aggregate them. It produces the final decision from the collective voting from the decision of the individual learners. The BE classifier is an ensemble classifier that uses the collaborative approach of the bagging and decision tree



(DT). The BE classifier predictor is explicitly given as follows (Ho, 1995):

$$F_{BE}^N(in, out) = \frac{1}{N} \sum_{i=1}^N T_i(in, out) \quad (16)$$

where  $(in, out)$  is the input–output set,  $N$  is the number of individual learners, and  $T$  is a single learner built from a subset of  $(in, out)$  by the bagging technique (Breiman, 2001). This bagged form of multiple learners grows in parallel and mitigates the limitations due to overfitting data with a single decision tree. The majority voting from the different bags is considered best suitable for the test set and is performed as follows:

$$S(in, out) = \arg \max_{out} \left( \sum_{i=1}^N f(out = T_i(in, out)) \right) \quad (17)$$

Here,  $f(out = T_i(in, out)) = 1$  for  $out = T_i(in, out)$  is true; otherwise,  $f(out = T_i(in, out)) = 0$ .

## 4 Results and discussion

The performance of the proposed protection scheme is tested on numerous possible fault cases (= 6000 cases) simulated on the two-bus system (Figure 1) by varying different parameters as listed in Table 1. The data are generated at a sampling frequency of 1 kHz. Results of some typical fault and non-fault cases are demonstrated in the following.

### 4.1 Results of the proposed fault detection algorithm

#### 4.1.1 Balanced fault

Results of a 3ph-fault initiated at 0.605 s with  $L_{f=}$  240 km away from relay  $R_G$  of Figure 1,  $FIA = 90^\circ$ ,  $CL = 40\%$ , and  $v = 10$  m/s are shown in Figure 7. As seen in the figure, the half-cycle magnitude differences of the line end positive-sequence currents ( $\Delta I_{1G}, \Delta I_{1W}$ )

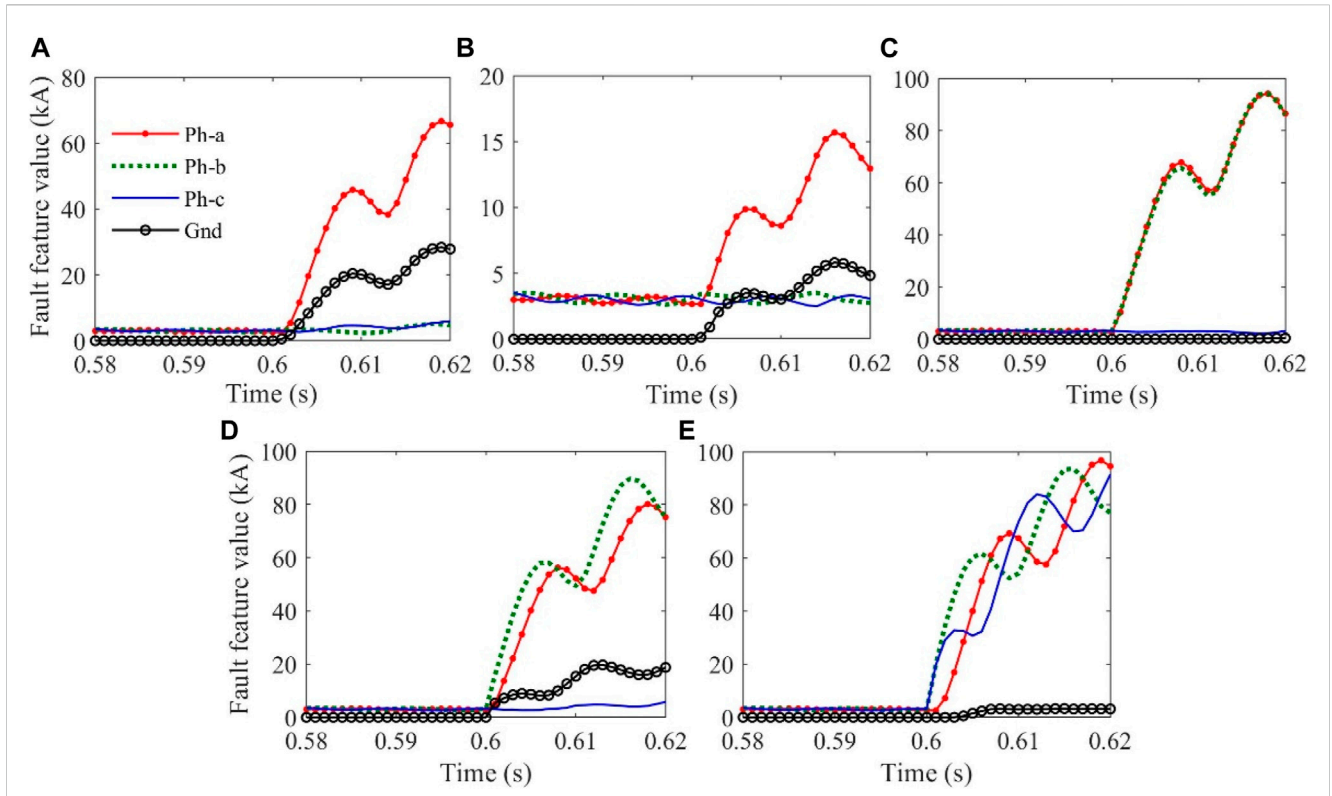


**FIGURE 11**  
 Demonstration of the variation of input fault features  $\beta$  to the BE classifier for few typical fault cases initiated at 0.6 s (60 km away from the grid side of Figure 1 with  $CL = 40\%$ ): (A) ag-fault ( $R_f = 10 \Omega$ ), (B) ag-fault ( $R_f = 200 \Omega$ ), (C) ab-fault, (D) abg-fault ( $R_f = 10 \Omega$ ), and (E) abc-fault.

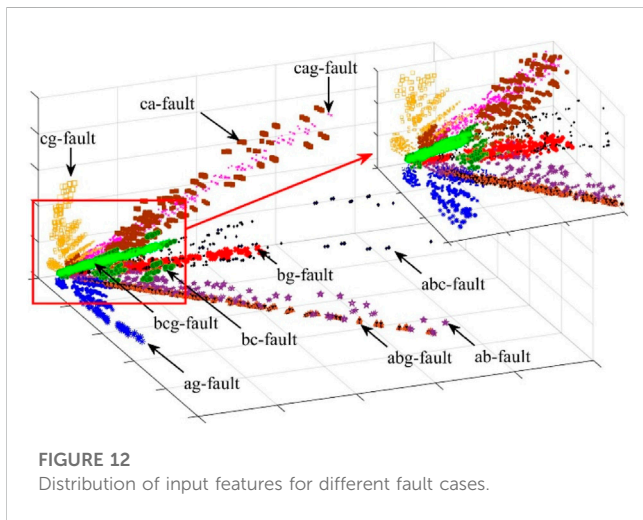


**FIGURE 12**  
 Distribution of input features for different fault cases.

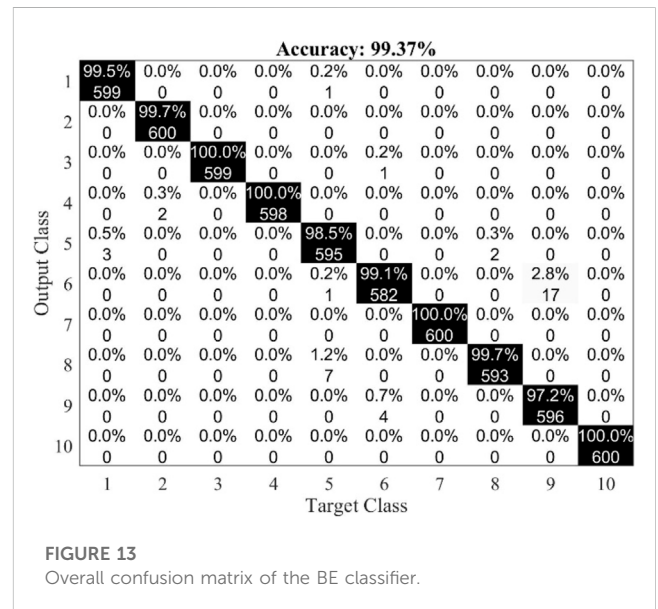


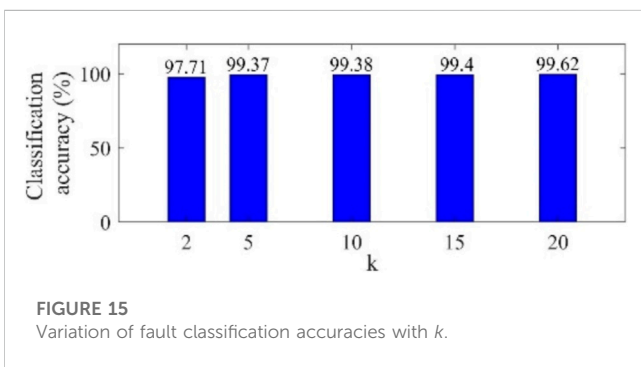
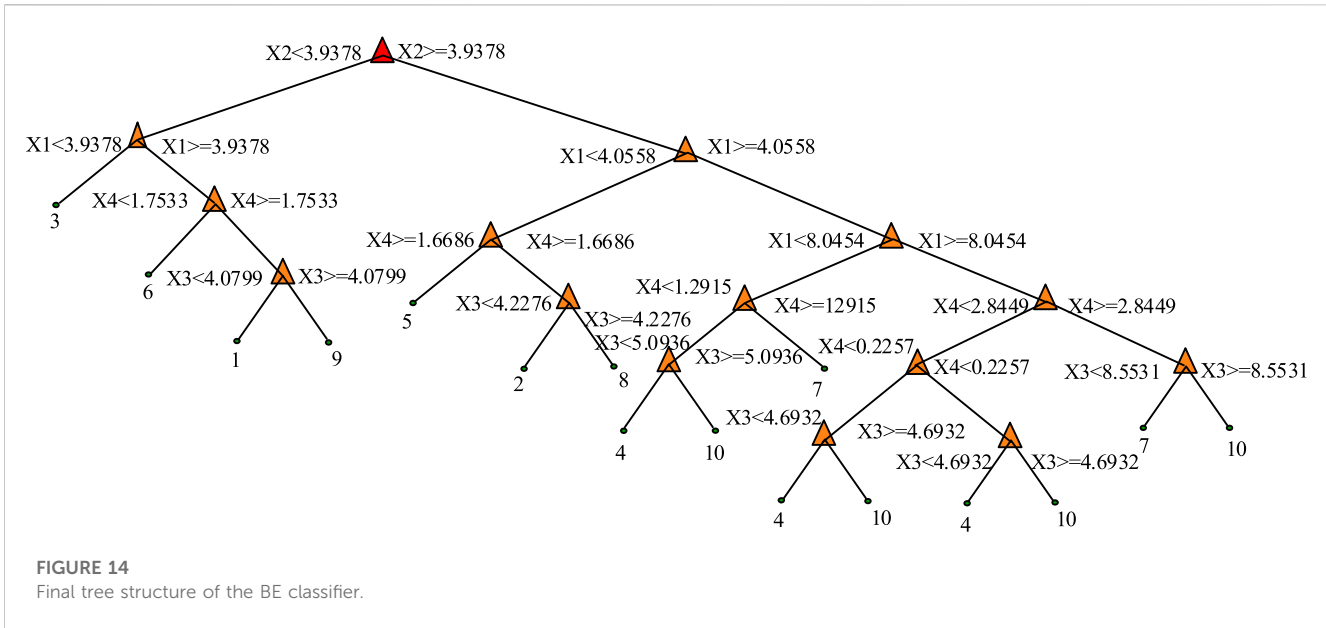
**FIGURE 13**  
 Overall confusion matrix of the BE classifier.

are of opposite signs, confirming the case of an internal fault in 3 ms only. Considering the 5 ms latency of the PLCC, the FDU activates the fault classification unit (FCU) in 8 ms.

### 4.1.2 Unbalanced fault

Performance is demonstrated for two different unbalanced faults: 1) an ag-fault initiated at 0.6 s ( $L_f = 270$  km (90% length

of the line) away from  $R_G$  with  $R_f = 10 \Omega$ ,  $FIA = 0^\circ$ ,  $CL = 40\%$ , and  $v = 5$  m/s) and 2) a bc-fault initiated at 0.605 s ( $L_f = 210$  km (70% length of the line) away from  $R_G$  with  $FIA = 90^\circ$ ,  $CL = 40\%$ , and  $v = 15$  m/s. Results of the previous three fault cases are shown in Figures 8A,B,



respectively. It is evident from Figure 8A that for all the unbalanced fault cases, signs of  $\Delta I_{IG}$  and  $\Delta I_{IW}$  are coming from the opposite direction. Thus, all three fault cases are internal faults in 8 ms and 3 ms, respectively. Including 5 ms PLCC latency, the FDU for these three fault cases activates the FCU after 13 ms and 8 ms, respectively.

### 4.1.3 High-resistance fault

Fault detection during high fault resistance is often difficult due to the possibility of minimal changes in the current magnitude. To test the efficacy during such fault situations, a bg-fault is initiated at 0.61 s with  $L_f = 240$  km away from  $R_G$ ,  $R_f = 200 \Omega$ ,  $FIA = 180^\circ$ ,  $CL = 70\%$ , and  $v = 10$  m/s. Despite high fault resistance, the signs of  $\Delta I_{IG}$  and  $\Delta I_{IW}$  are opposite, and the proposed FDU detects and activates the FCU in 10 ms considering the 5 ms latency of PLCC (Figure 8B).

### 4.1.4 Performance during three-phase fault producing current transformer saturation

Sometimes, the core of the CT is saturated due to severe short circuit faults and the burden settings of the CT. In such a situation, the secondary currents of the CTs may not be replicated correctly as those of the primary currents. Due to the incorrect secondary current during CT saturation, the relay may find difficulty in correctly distinguishing

internal faults from external faults. To test the performance during such a situation, a three-phase fault is created at 0.603 s with  $L_f = 210$  km (70% length of the line) away from  $R_G$  while  $FIA = 54^\circ$ ,  $CL = 40\%$ , and  $v = 15$  m/s. Here, the burden of grid-side CTs is chosen in such a way that the CT secondary current referred to as primary defers from the actual current, as shown in Figure 9A. The B-H curves of the three CTs shown in Figure 9B also confirm that the CT cores are saturated. Despite the CT saturation, the signs of the superimposed positive-sequence currents at Bus-G and Bus-W are opposite in polarity, and the proposed FDU detects and activates the FCU in 10 ms, considering 5 ms latency of PLCC. Thus, CT saturation is not an issue for the proposed fault detection algorithm.

### 4.1.5 Non-fault transients

The fault detector should remain silent during non-fault transients such as capacitor switching, load switching, and noise. Results during the initiation of three non-fault transients: 1) switching of a capacitor equivalent to 40% MVAR capacity of the line, 2) a load of 50% capacity of the total MW demand is switched on suddenly, and 3) the presence of noise in the current waveform with a signal-to-noise ratio of 15 db. During the initiation of the previous three non-fault transients, the wind speed was maintained at 15 m/s. As observed from the results (Figures 10A–C), the present fault detection scheme remains silent during the initiation of all the three non-fault transients.

## 4.2 Efficacy testing of the proposed fault classification scheme

The present work captures the current data for 6000 fault cases simulated in Figure 1 through MATLAB/Simulink® by changing the different parameters, as shown in Table 1. From the one-cycle post-fault three-phase current signals of all the generated fault cases, the valuable features are extracted using FBSE and SVD first. Out of the total generated data cases, 70% and 30% of the feature data cases are then used to train and test the BE classifier, respectively. The

TABLE 2 Comparative assessment result.

Parameter	Swetapadma et al. (2017)	Mohammad Taheri et al. (2018)	Mishra et al. (2019)	Prasad et al. (2020)	Proposed method
Method used	DWT, k-NN	DPASC, DT	FDOST, DT	PSO	FBSE, SVD, BE
System and sampling frequency	50 Hz & 1 kHz	50 Hz & 1 kHz	50 Hz & 1 kHz	60 Hz & 1.2 kHz	50 Hz & 1 kHz
Data utilized	Current	Differential current	Voltage and current	Differential current	Current
Network consists of	FSC	FSC	FSC	Wind farm	FSC, Wind farm
Fault detection accuracy in %	100	100	99.9	NM	100
Fault classification accuracy in %	100	100	99.9	NM	100
Delay time in ms	<10	<10	<10	NM	<10
Max. $R_f$ in $\Omega$	100	300	200	NM	200
Affected by high $R_f$	No	No	No	No	No
Is it affected by CT saturation?	NM	NM	No	NM	No
Is it affected by load switching?	NM	NM	NM	NM	No
Affected by capacitor switching?	NM	NM	NM	NM	No
Affected by current inversion?	NM	NM	NM	NM	No
Affected by noise?	NM	NM	No	NM	No
Real-time validation	NM	NM	NM	NM	OPAL-RT

NM, not mentioned.

variations of the input fault feature  $\beta$  to the BE classifier for a few faults generated in Figure 1 are shown in Figure 11. With the initiation of faults, the fault features  $\beta$  of the faulted phase are increased from a lower value to a higher value, making a more straightforward estimation of fault types by the BE classifier.

The scatter plot of all the 6000-feature data generated, as demonstrated in Figure 12, clearly shows different feature datasets for different fault cases. The computed overall confusion matrix (Figure 13) shows that the classification accuracy of the proposed BE classifier for fault classification is 99.37%. Figure 14 shows the final tree structure of the BE classifier.

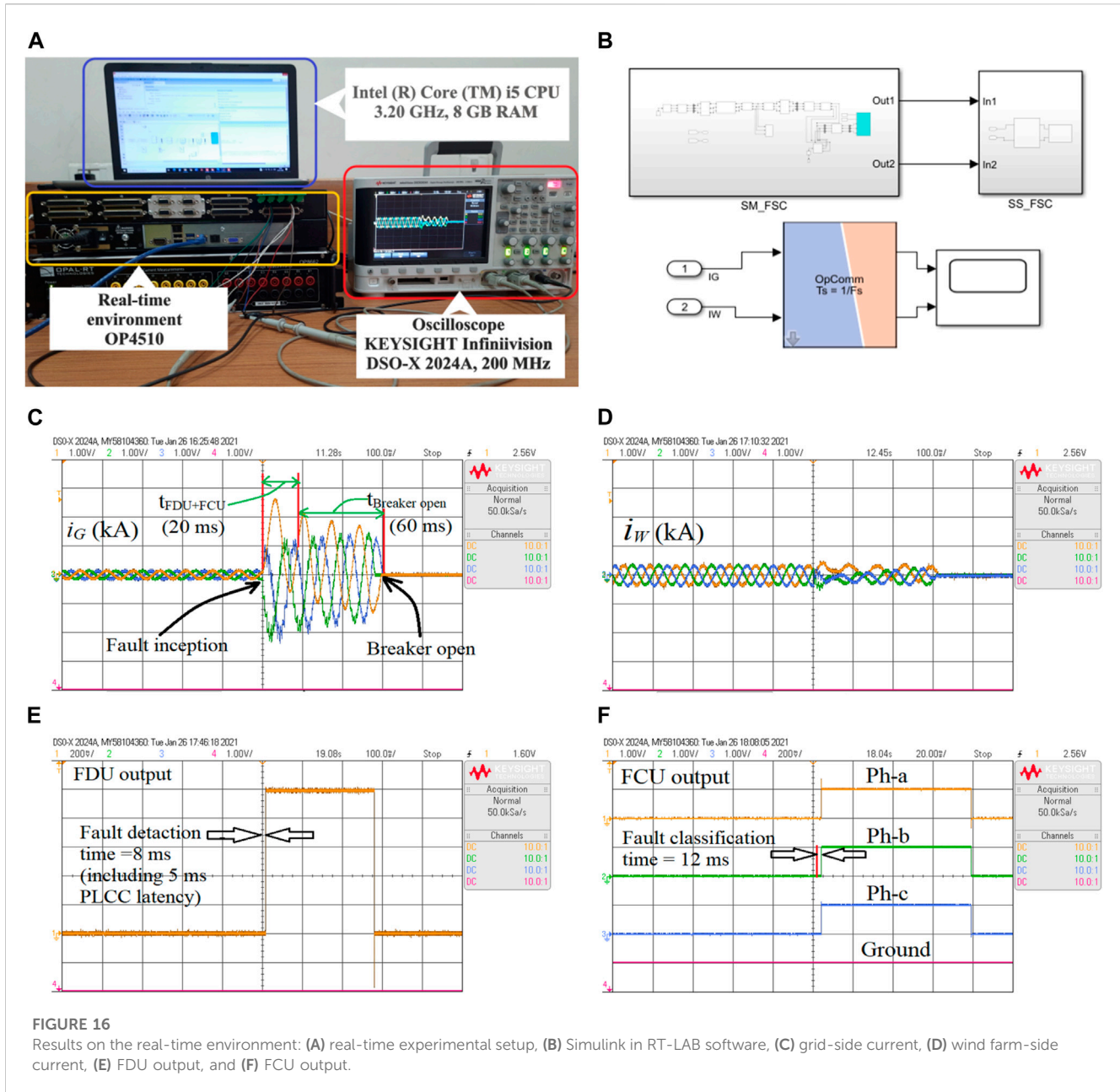
In the present work,  $k$ -fold cross-validation is used to counteract the bias-variance problem. Here, the  $k$ -fold cross-validation uses  $k = 2, 5, 10, 15,$  and  $20$ . As evident from Figure 15, after  $k = 5$ , there is no such improvement in the classification accuracy. Thus, to avoid computational complexity and time, fault classification accuracy is calculated using  $k = 5$ .

## 5 Comparative assessment

The performance of the proposed method is compared with Prasad et al. (2020), Mishra et al. (2019), Swetapadma et al. (2017), and Mohammad Taheri et al. (2018) earlier used for the protection of either FSC-compensated TLs or DFIG wind farm-connected TLs.

The summarized comparative study considering different attributes is provided in Table 2. The table clearly shows that the proposed approach's fault detection and classification accuracies are coming 100%. Similar accuracies are obtained earlier by Swetapadma et al. (2017) and Mohammad Taheri et al. (2018). However, the methods proposed by Swetapadma et al. (2017) and Mohammad Taheri et al. (2018) are tested only for FSC-compensated TLs. These protection schemes were not validated for large-scale DFIG wind farm integration. The control action of DFIG with LVRT capability and the grounding arrangement of DFIG produce unusual frequency components and unusual sequence currents, especially during ground faults. These characteristics will affect the performance of the existing methods.

Furthermore, the discrete wavelet transforms (DWTs),  $k$ -nearest neighbor ( $k$ -NN)-based method used in the study by Swetapadma et al. (2017), differential phase angle of superimposed current (DPASC), and DT-based method used in the study by Mohammad Taheri et al. (2018) are computationally not efficient compared to the proposed FBSE-SVD and BE classifier. Also, the methods proposed by Swetapadma et al. (2017) and Mohammad Taheri et al. (2018) have not been tested in the presence of non-fault transients such as significant load switching, switching on/off of capacitor banks, and CT saturation during severe short circuit faults. The method in the study by Mohammad Taheri et al. (2018) used the current differential principle. Such a scheme cannot ensure secure protection for TLs connecting large-scale DFIG



wind farms. The performance of the proposed protection scheme has immunity to such non-fault transients. This shows that the overall performance of the proposed protection scheme is superior compared to that the existing approaches, mainly when used for the protection of FSC-compensated TLs connected with large-scale DFIG wind farms.

## 6 Real-time validation through the OPAL-RT platform

The proposed protection scheme is tested on the RTDS platform manufactured by OPAL-RT (OP4510). The experimental setup is shown in Figure 16A (Biswas et al., 2022). As shown in Figure 16B, the test model of Figure 1 is simulated in MATLAB/Simulink<sup>®</sup> and compiled in RT-Lab software. The real-

time data are generated and stored in the processor of OP4510. The real-time current at the grid side for a 3ph-fault ( $L_f = 240$  km from relay  $R_G$ ,  $CL = 70\%$ ,  $v = 5$  m/s) provided in Figure 16C shows the fault detection and classification time of the proposed method is 20 ms. The real-time current at the wind farm site for the previous fault case is shown in Figure 16D. Considering 60 ms circuit breaker operating time, the faulted phases are finally tripped in 80 ms (Figures 16E,F). This shows that the proposed protection scheme can be implemented easily in real-time.

## 7 Conclusion

In the present paper, the limitations of distance relay protecting an FSC-compensated TL connecting large-capacity

DFIG-WTGs are studied, and an intelligent protection scheme is proposed for fast and reliable detection and classification of faults in such crucial TLs. The proposed scheme utilizes the signs of the half-cycle magnitude differences of the line-end positive-sequence currents for fault detection, and the fault classification is performed using the local current measurements processed through the combination of the FBSE-SVD-BE classifier. Performance is evaluated on 6000 fault cases simulated on the two-bus test system through MATLAB/Simulink<sup>®</sup>. The method is also validated in OPAL-RT (OP4510) manufactured RTDS platform. The marginal computational burden, feasibility for real-time implementation, fast fault detection and classification time (<10 ms), 100% fault detection accuracies, and comparatively higher fault classification accuracies (= 99.37% are the main merits of the proposed relaying algorithm. However, the proposed approach's efficacy is validated through the OPAL-RT-manufactured RTDS platform. It must be validated through the hardware-in-loop (HIL) experimental setup using OPAL-RT systems and field-programmable gate array (FPGA) boards with prototype relays and should be compared with existing relays used in fields such as SEL-421. This may be extended as future work.

## Data availability statement

The original contributions presented in the study are included in the article/Supplementary Material; further inquiries can be directed to the corresponding author.

## References

- Abdelaziz, A. Y., Ibrahim, A. M., Mansour, M. M., and Talaat, H. E. (2005). Modern approaches for protection of series compensated transmission lines. *Electr. Power Syst. Res.* 75 (1), 85–98. doi:10.1016/j.epr.2004.10.016
- Altuve, H. J., Mooney, J. B., and Alexander, G. E. (2009). "Advances in series-compensated line protection," in 62nd Annual Conf. for Protective Relay Engineers, College Station, TX, USA, 30 March 2009 - 02 April 2009 (IEEE), 263–275.
- Biswas, S., and Nayak, P. K. (2021). A fault detection and classification scheme for unified power flow controller compensated transmission lines connecting wind farms. *IEEE Syst. J.* 15 (1), 297–306. doi:10.1109/jsyst.2020.2964421
- Biswas, S., and Nayak, P. K. (2019). An unblocking assistance to distance relays protecting TCSC compensated transmission lines during power swing. *Int. Trans. Electr. Energy Syst.* 29 (8), 1–21. doi:10.1002/2050-7038.12034
- Biswas, S., and Nayak, P. K. (2021). A new approach for protecting TCSC compensated transmission lines connected to DFIG-based wind farm. *IEEE Trans. Indus. Infor.* 17 (8), 5282–5291. doi:10.1109/tii.2020.3029201
- Biswas, S., Nayak, P. K., and Pradhan, G. (2022). A dual-time transform assisted intelligent relaying scheme for the STATCOM-compensated transmission line connecting wind farm. *IEEE Syst. J.* 16 (2), 2160–2171. doi:10.1109/jsyst.2021.3070448
- Breiman, L. (2001). Random forests. *Mach. Learn.* 45 (1), 5–32. doi:10.1023/a:1010933404324
- Sahoo, B., and Samantaray, S. R. (2017). An enhanced fault detection and location estimation method for TCSC compensated line connecting wind farm. *Int. J. Electr. Power Energy Syst.* 96, 432–441. doi:10.1016/j.ijepes.2017.10.022
- Central Electricity Regulatory Commission (2010). Indian electricity grid code. Available: [http://cercind.gov.in/2010/ORDER/February2010/IEGC\\_Review\\_Proposal.pdf](http://cercind.gov.in/2010/ORDER/February2010/IEGC_Review_Proposal.pdf).
- Chaurasiya, P. K., Warudkar, V., and Ahmed, S. (2019). Wind energy development and policy in India: A review. *Energy Strategy Rev.* 24, 342–357. doi:10.1016/j.esr.2019.04.010
- Chen, S., Tai, N., Fan, C., Liu, J., and Hong, S. (2017). Adaptive distance protection for grounded fault of lines connected with doubly-fed induction generators. *IET Gener. Transm. Distrib.* 11 (6), 1513–1520. doi:10.1049/iet-gtd.2016.1145
- Chen, S., Yin, X., and Zhang, Z. (2017). Impacts of DFIG-based wind farm integration on its tie line distance protection and countermeasures. *IEEE Trans. Electr. Electron. Eng.* 12 (4), 553–564. doi:10.1002/tee.22411
- Dash, P. K., Samantaray, S. R., and Panda, G. (2006). Fault classification and section identification of an advanced series-compensated transmission line using support vector machine. *IEEE Trans. Power Deliv.* 22 (1), 67–73. doi:10.1109/tpwr.2006.876695
- D'Elia, G., Delvecchio, S., and Dalpiaz, G. (2012). "On the use of Fourier-Bessel series expansion for gear diagnostics," in *Condition monitoring of machinery in non-stationary operations* (Berlin, Germany: Springer), 267–275.
- Dubey, R. K., Samantaray, S. R., and Panigrahi, B. K. (2014). Adaptive distance relaying scheme for transmission network connecting wind farms. *Electr. Power Compon. Syst.* 42 (11), 1181–1193. doi:10.1080/15325008.2014.921953
- Fang, Y., Jia, K., Yang, Z., Li, Y., and Bi, T. (2018). Impact of inverter-interfaced renewable energy generators on distance protection and an improved scheme. *IEEE Trans. Ind. Electron.* 66 (9), 7078–7088. doi:10.1109/tie.2018.2873521
- Fortescue, C. L. (1918). Method of symmetrical co-ordinates applied to the solution of polyphase networks. *Trans. Am. Inst. Electr. Eng.* 21 (2), 1027–1140. doi:10.1109/t-aiee.1918.4765570
- Ghorbani, A., Mehrjerdi, H., and Al-Emadi, N. A. (2017). Distance-differential protection of transmission lines connected to wind farms. *Int. J. Electr. Power Energy Syst.* 89, 11–18. doi:10.1016/j.ijepes.2017.01.002
- Gopalan, K., Anderson, T. R., and Cupples, E. J. (1997). "Speaker identification using features based on first-order Bessel function expansion of speech," in IEEE Pacific Rim Conference on Communications, Computers and Signal Processing, 10 Years Networking the Pacific Rim, 1987-1997, Victoria, BC, Canada, 20-22 August 1997 (IEEE), 589–592.
- Gopalan, K. (2001). "Speech coding using Fourier-Bessel expansion of speech signals," in 27th Annual Conf. of the IEEE Indus. Electronics Society (Cat. No.

## Author contributions

PM simulated the system and generated the data for training and testing the Fourier–Bessel series expansion (FBSE) bagging ensemble (BE) classifier for performing the fault classification task. He also wrote the initial draft of the manuscript. SB studied and tested the simultaneous impacts of the installation of series compensation and the integration of large-scale wind farms on distance relay performance. He also wrote the initial draft of Section 2 of the manuscript. PN edited the whole manuscript. AA provided guidance for the overall improvement of the manuscript. AS provided further guidance for the overall improvement of the manuscript.

## Conflict of interest

The authors declare that the research was conducted in the absence of any commercial or financial relationships that could be construed as a potential conflict of interest.

## Publisher's note

All claims expressed in this article are solely those of the authors and do not necessarily represent those of their affiliated organizations, or those of the publisher, the editors, and the reviewers. Any product that may be evaluated in this article, or claim that may be made by its manufacturer, is not guaranteed or endorsed by the publisher.

- 37243), Denver, CO, USA, 29 November 2001 - 02 December 2001 (IEEE), 2199–2203.
- Ho, T. K. (1995). Random decision forests. In Proceedings of 3rd international conference on document analysis and recognition. Montreal, QC, Canada, 14–16 August 1995, IEEE, 278–282.
- Hoang, T. T., Tran, Q. T., Le, H. S., Nguyen, H. N., and Duong, M. Q. (2022). “Impacts of high solar inverter integration on performance of FLIRS function: Case study for Danang distribution network,” in 2022 11th International Conference on Control, Automation and Information Sciences (ICCAIS) (Hanoi, Vietnam: IEEE), 327–332.
- Hooshyar, A., Azzouz, M. A., and El-Saadany, E. F. (2014). Distance protection of lines connected to induction generator-based wind farms during balanced faults. *IEEE Trans. Sustain. Energy* 5 (4), 1193–1203. doi:10.1109/tste.2014.2336773
- Hoq, M. T., Wang, J., and Taylor, N. (2021). Review of recent developments in distance protection of series capacitor compensated lines. *Electr. Power Syst. Res.* 190, 106831. doi:10.1016/j.epsr.2020.106831
- Li, B., Liu, J., Wang, X., and Zhao, L. (2018). Fault studies and distance protection of transmission lines connected to DFIG-based wind farms. *Appl. Sci.* 8 (4), 562. doi:10.3390/app8040562
- Lopez, J., Gubia, E., Sanchis, P., Roboam, X., and Marroyo, L. (2008). Wind turbines based on doubly fed induction generator under asymmetrical voltage dips. *IEEE Trans. Energy Convers.* 23 (1), 321–330. doi:10.1109/tec.2007.914317
- Lopez, J., Sanchis, P., Roboam, X., and Marroyo, L. (2007). Dynamic behavior of the doubly-fed induction generator during three-phase voltage dips. *IEEE Trans. Energy Convers.* 22 (3), 709–717. doi:10.1109/tec.2006.878241
- Ma, J., Zhang, W., Liu, J., and Thorp, J. S. (2018). A novel adaptive distance protection scheme for DFIG wind farm collector lines. *Int. J. Electr. Power Energy Syst.* 94, 234–244. doi:10.1016/j.ijepes.2017.07.008
- Mishra, P. K., Yadav, A., and Pazoki, M. (2018). A novel fault classification scheme for series capacitor compensated transmission line based on bagged tree ensemble classifier. *IEEE Access* 6, 27373–27382. doi:10.1109/access.2018.2836401
- Mishra, P. K., Yadav, A., and Pazoki, M. (2019). FDOST-based Fault Classification scheme for fixed series compensated transmission system. *IEEE Syst. J.* 13 (3), 3316–3325. doi:10.1109/jsyst.2018.2890288
- Mishra, S., Gupta, S., and Yadav, A. (2021). A novel two-terminal fault location approach utilizing traveling-waves for series compensated line connected to wind farms. *Elect. Power Syst. Res.* 198, 107362. doi:10.1016/j.epsr.2021.107362
- Mohamed, A. R., Sharaf, H. M., and Ibrahim, D. K. (2021). Enhancing distance protection of long transmission lines compensated with TCSC and connected with wind power. *IEEE Access* 9, 46717–46730. doi:10.1109/access.2021.3067701
- Mohammad Taheri, M., Seyedi, H., Nojavan, M., Khoshbouy, M., and Ivatloo, B. M. (2018). High-speed decision tree-based series-compensated transmission lines protection using differential phase angle of superimposed current. *IEEE Trans. Power Deliv.* 33 (6), 3130–3138. doi:10.1109/tpwrd.2018.2861841
- Nayak, P. K., Pradhan, A. K., and Bajpai, P. (2014). Wide-area measurement-based backup protection for power network with series compensation. *IEEE Trans. Power Deliv.* 29 (4), 1970–1977. doi:10.1109/tpwrd.2013.2294183
- Nayak, S., Kar, S. K., Dash, S. S., Vishnuram, P., Thanikanti, S. B., and Nastasi, B. (2022). Enhanced salp swarm algorithm for multimodal optimization and fuzzy based grid frequency controller design. *Energies* 15 (9), 3210. doi:10.3390/en15093210
- Novosel, D., Phadke, A., Saha, M. M., and Lindahl, S. (1997). “Problems and solutions for microprocessor protection of series compensated lines,” in Sixth International Conference on Developments in Power System Protection, Nottingham, UK, 25–27 March 1997 (IEEE), 18–23.
- Ouyang, J., and Xiong, X. (2014). Dynamic behavior of the excitation circuit of a doubly-fed induction generator under a symmetrical voltage drop. *Renew. Energy* 71, 629–638. doi:10.1016/j.renene.2014.06.029
- Pachori, R. B., and Sircar, P. (2008). EEG signal analysis using FB expansion and second-order linear TVAR process. *Signal Process.* 88 (2), 415–420. doi:10.1016/j.sigpro.2007.07.022
- Pazoki, M. (2018). A new fault classifier in transmission lines using intrinsic time decomposition. *IEEE Trans. Ind. Inf.* 14 (2), 619–628. doi:10.1109/tii.2017.2741721
- Pradhan, A. K., and Joos, G. (2007). Adaptive distance relay setting for lines connecting wind farms. *IEEE Trans. Energy Convers.* 22 (1), 206–213. doi:10.1109/tec.2006.889621
- Prasad, C. D., Biswal, M., and Abdelaziz, A. Y. (2020). Adaptive differential protection scheme for wind farm integrated power network. *Electr. Power Syst. Res.* 187, 106452. doi:10.1016/j.epsr.2020.106452
- Prasad, C. D., and Biswal, M. (2020). Swarm intelligence-based differential protection scheme for wind integrated transmission system. *Comput. Electr. Eng.* 86, 106709. doi:10.1016/j.compeleceng.2020.106709
- Sadeghi, H. (2012). A novel method for adaptive distance protection of transmission line connected to wind farms. *Int. J. Electr. Power Energy Syst.* 43 (1), 1376–1382. doi:10.1016/j.ijepes.2012.06.072
- Schroeder, J. (1993). Signal processing via Fourier-Bessel series expansion. *Digit. Signal Process.* 3 (2), 112–124. doi:10.1006/dspr.1993.1016
- Sivov, O., Abdelsalam, H., and Makram, E. (2016). Adaptive setting of distance relay for MOV-protected series compensated line considering wind power. *Electr. Power Syst. Res.* 137, 142–154. doi:10.1016/j.epsr.2016.03.048
- Swetapadma, A., Mishra, P., Yadav, A., and Abdelaziz, A. Y. (2017). A non-unit protection scheme for double circuit series capacitor compensated transmission lines. *Electr. Power Syst. Res.* 148, 311–325. doi:10.1016/j.epsr.2017.04.002
- Tikhonov, A. N. (1963). Solution of incorrectly formulated problems and the regularization method. *Sov. Math.* 4, 1035–1038.
- Tran, V. T., Al Thobiani, F., Ball, A., and Choi, B.-K. (2013). An application to transient current signal-based induction motor fault diagnosis of Fourier-Bessel expansion and simplified fuzzy ARTMAP. *Expert Syst. Appl.* 40 (13), 5372–5384. doi:10.1016/j.eswa.2013.03.040
- Varma, R. K., Auddy, S., and Semsedini, Y. (2008). Mitigation of subsynchronous resonance in a series-compensated wind farm using FACTS controllers. *IEEE Trans. Power Del.* 23 (3), 1645–1654. doi:10.1109/tpwrd.2008.917699
- Varma, R. K., and Moharana, A. (2013). SSR in double-cage induction generator-based wind farm connected to series-compensated transmission line. *IEEE Trans. Power Syst.* 28 (3), 2573–2583. doi:10.1109/tpwrs.2013.2246841
- Vishnuram, P., Ramchandiran, G., Sudhakar, T. B., and Nastasi, B. (2021). Induction heating in domestic cooking and industrial melting applications: A systematic review on modelling, converter topologies and control schemes. *Energies* 14 (20), 6634–34. doi:10.3390/en14206634
- Vyas, B., Maheshwari, R. P., and Das, B. (2014). Protection of series compensated transmission line: Issues and state of art. *Electr. Power Syst. Res.* 107, 93–108. doi:10.1016/j.epsr.2013.09.017
- Xiao, F., Zhang, Z., and Yin, X. (2015). Fault current characteristics of the DFIG under asymmetrical fault conditions. *Energies* 8 (10), 10971–10992. doi:10.3390/en81010971
- Yang, Z., Jia, K., Fang, Y., Zhu, Z., Yang, B., and Bi, T. (2020). High-frequency fault component-based distance protection for large renewable power plants. *IEEE Trans. Power Electron.* 35 (10), 10352–10362. doi:10.1109/tpel.2020.2978266



## Appendix

### Parameters of the grid transmission line:

TL length: 300 km.

Positive-sequence impedance ( $Z_1$ ):  $0.03293 + j0.327 \Omega/\text{km}$ .

Zero-sequence impedance ( $Z_0$ ):  $0.2587 + j1.1740 \Omega/\text{km}$ .

Positive-sequence capacitive impedance:  $280.1 \text{ M}\Omega/\text{km}$ .

Zero-sequence capacitive reactance:  $461.2546 \text{ M}\Omega/\text{km}$ .

### Parameters of DFIG wind farm:

Rating of wind farm: 0.690 kV, 50 Hz, 60 MW, 28 MVA<sub>r</sub> (40 Nos.  $\times$  2 MW each), slip =  $-0.25$ , and inertia constant: 4.32.

Collector lines: 30 km  $\pi$ -section,  $Z_1 = 0.115 + j0.33 \Omega/\text{km}$ .

Transformer before collector line Y/ $\Delta$ , 2.2 MVA, 0.690/35 kV, 50 Hz.

Transformer after collector line  $\Delta$ /Y, 90 MVA, 35/400 kV, 50 Hz.

### Parameters of the capacitor bank:

Capacitance:  $80 \mu\text{F}$  (40% compensation),  $45 \mu\text{F}$  (70% compensation); MOV voltage: 75 kV.